ChemComm

COMMUNICATION

View Article Online
View Journal | View Issue

Cite this: *Chem. Commun.*, 2023, 59, 13767

Received 6th September 2023,
Accepted 24th October 2023

DOI: 10.1039/d3cc04409b

rsc.li/chemcomm

Bifunctional CoFe/HZSM-5 catalysts orient CO_2 hydrogenation towards liquid hydrocarbons†

Kai Wang,[ab] Na Liu,[ab] Jian Wei,* [a] Yang Yu,[ab] Jixin Zhang,[a] Joshua Iseoluwa Orege,[ab] Lifei Song,[a] Qingjie Ge [a] and Jian Sun *[a]

Converting CO_2 to liquid (C_{5+}) hydrocarbons remains a significant hurdle. Our study shows that CoFe/HZSM-5 boosts C_{5+} selectivity to 73.4%, up from 59% for Fe/HZSM-5. This study highlights the pivotal roles of zeolite acidity and catalyst proximity in this improvement. These insights pave the way for more effective CO_2 utilization.

The hydrogenation of CO_2 into valuable chemicals such as aromatics and olefins presents an effective approach for addressing the rising CO_2 levels, transforming the greenhouse gas into beneficial resources. This process holds potential in mitigating CO_2 emissions and converting CO_2 into a sought-after commodity.[1]

Despite challenges such as CO_2's inert nature and high energy barriers for C–C coupling,[2] there are two main approaches for CO_2 hydrogenation into long-chain hydrocarbons: the methanol-mediated (CO_2-MeOH) route and the CO_2 modified Fischer–Tropsch synthesis (CO_2-FTS) route. The CO_2-MeOH route, despite yielding a higher proportion of low carbon olefins or liquid (C_{5+}) hydrocarbons, has limitations like low CO_2 conversion and increased CO selectivity.[3,4] The CO_2-FTS route involves CO_2 transformation into CO intermediates through reverse water–gas shift (RWGS) and further conversion to C_{2+} products *via* the FTS process.[5] Co- and Fe-based catalysts are widely used in the FTS route.[6] While the Fe-based catalysts are effective for both RWGS and FTS processes, the Co-based catalysts often show inefficiency due to their lack of RWGS reactivity.[7] Enhancing the performance of the Co-based catalysts with active sites for the RWGS reaction improves the overall process. Specific studies have seen success by integrating noble metals or alkali metals into the Co-based catalysts, leading to a reduced CO_2 conversion rate but augmented production of long-chain hydrocarbons.[8]

In recent years, researchers have developed multi-active-site synergistic catalysts by pairing metal catalysts with zeolites for CO_2 hydrogenation.[5] Zeolites, unique in their topological structures and acidic properties, aid in hydrocarbon reactions like oligomerization and isomerization.[9] After CO_2 transforms into olefins *via* the metal catalyst, it is further converted to higher carbon hydrocarbons on the zeolites.[10] The ZSM-5 zeolite framework consists of interconnected 10-membered rings, creating a three-dimensional microporous channel structure.[11] These channels provide a large surface area and space for molecular diffusion,[12,13] making ZSM-5 more resistant to coking compared to other zeolites due to its pore system constraints.[14]

In our recent work, we found that CoFe alloy carbide catalysts excel in converting CO_2 to olefins,[15] which are key intermediates in the CO_2-FTS route. Enhancing olefin selectivity is a strategic move, as it inherently augments the selectivity of C_{5+} hydrocarbons in subsequent reactions. CoFe alloy catalysts, with their exemplary capability to catalyse the transformation of CO_2 into olefins, can bolster the system's proficiency in CO_2 conversion to C_{5+} hydrocarbons.[16] With this premise, our explorations have delved into the integration of ZSM-5 zeolites, exhibiting varied acidity characteristics, with CoFe alloy catalysts. This paper seeks to present a comprehensive study of the CO_2 hydrogenation performance steered by this tandem catalytic system and decipher the underlying mechanisms influenced by zeolite acidity and the nuanced interplay between the zeolite and metal catalyst.

The crystal structures of each component in the tandem catalyst system were characterized using X-ray diffraction (XRD) analysis. The fresh CoFe catalyst displayed distinct peaks at 2θ = 36.8° and 48.5°, matching the $CoFe_2O_4$ phase (Fig. S1, PDF #22-1086, ESI†),[17] while the spent catalyst revealed $(Co_xFe_{1-x})_5C_2$ alloy carbide, the key active centre for CO_2 hydrogenation (Fig. S2, ESI†). These results align with our previous studies on CoFe catalysts.[18] Hydrothermally-synthesized HZSM-5 zeolites (see the details in the ESI†) are denoted as HZ-5(*X*), where *X*

[a] *Dalian National Laboratory for Clean Energy, Dalian Institute of Chemical Physics, Chinese Academy of Sciences, Dalian 116023, China. E-mail: weijian@dicp.ac.cn, sunj@dicp.ac.cn*

[b] *University of Chinese Academy of Sciences, Beijing 100049, China*

† Electronic supplementary information (ESI) available. See DOI: https://doi.org/10.1039/d3cc04409b

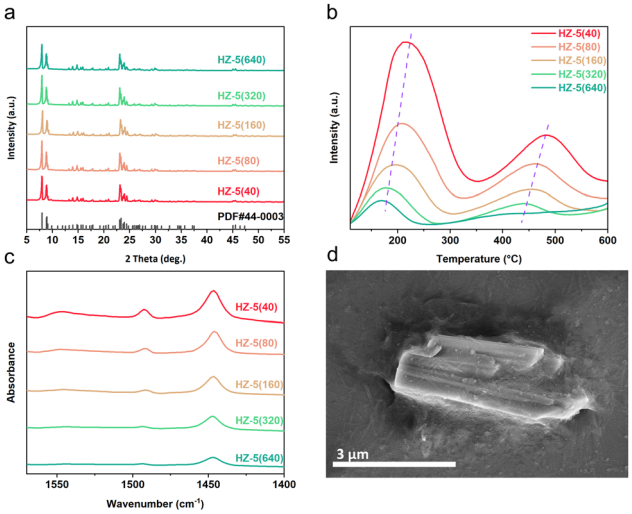

Fig. 1 (a) XRD patterns of HZSM-5 zeolites; (b) NH_3-TPD curves of HZSM-5 zeolites; (c) Py-IR spectra of HZSM-5 zeolites recorded after the removal of weakly adsorbed pyridine by evaporation at 200 °C; (d) SEM diagram of HZ-5(40).

corresponds to the SiO_2/Al_2O_3 ratio values: 40, 80, 160, 320, and 640. (A sample with a ratio of 20 was tested but quickly deactivated (Fig. S3, ESI†). Thus, we emphasized samples with higher ratios.) Their XRD patterns (Fig. 1a) showed peaks aligning closely with standard ZSM-5 (PDF #44-0003), confirming their high crystallinity and well-defined MFI topology.

The textural properties of CoFe were explored using N_2 adsorption–desorption experiments, revealing a mesoporous structure (Table S1, ESI†). The textural properties of HZSM-5 zeolites were investigated through N_2 adsorption–desorption experiments and scanning electron microscopy (SEM). The N_2 adsorption–desorption curves and textural properties of HZSM-5 zeolites with different SiO_2/Al_2O_3 ratios are shown in Fig. S4 (ESI†) and Table 1. All zeolites exhibited typical Type I isotherms, indicating their microporous structures. Moreover, variations in the SiO_2/Al_2O_3 ratio had a negligible influence on the structural properties of ZSM-5, as evident from the specific surface area and total pore volume. The SEM image in Fig. 1d reveals that the HZ-5(40) crystals are approximately 2–4 μm in size and exhibit a smooth surface, consistent with the zeolites having other SiO_2/Al_2O_3 ratios (Fig. S4, ESI†).

The acidity of HZSM-5 zeolites is pivotal in influencing the reactivity of tandem catalysts and hydrocarbon product selectivity. By employing NH_3-temperature-programmed desorption (NH_3-TPD) and pyridine adsorption infrared (Py-IR) techniques, the acidic properties were systematically characterized. The NH_3-TPD results showed desorption peaks at around 200 and 450 °C, representing weak and strong acidic sites, which decreased in intensity as the SiO_2/Al_2O_3 ratio increased from 40 to 640. Concurrently, the Py-IR spectra indicated a corresponding decline in Brønsted and Lewis acid site (BAS and LAS) concentrations, from 61.90 to 3.85 μmol g^{-1} for the BAS and 117.14 to 46.72 μmol g^{-1} for the LAS (Table 1). Both methods consistently suggest that increasing the SiO_2/Al_2O_3 ratio leads to reduced acid strength and concentration, attributable to the decreased aluminium content.

The CoFe alloy catalyst and HZSM-5 with different acidic properties were combined through particle mixing in a mass ratio of CoFe : HZSM-5 = 1 : 2 unless otherwise stated. After reducing and pretreating the catalyst at 350 °C under a H_2 atmosphere for 8 hours, its CO_2 hydrogenation performance was evaluated (Fig. 2a and b). The individual CoFe alloy catalyst achieved a CO_2 conversion rate of 39.0% with a CO selectivity of 11.3%, primarily producing olefins from CO_2 hydrogenation. It should be noted that both the CoFe and Fe catalysts used in this study were modified with sodium (Na) to enhance their catalytic performance,[19] enhancing their catalytic performance. CH_4 and straight-chain paraffins constituted a minor fraction of the hydrocarbon products, with the negligible formation of aromatics or iso-paraffins. When the CoFe alloy catalyst was combined with the HZ-5(40) zeolite, the tandem catalyst shifted the hydrocarbon profile significantly—olefins within C_{5+} fell from 68.5% to 1.0%, while aromatics and iso-paraffins surged from 0% and 11.3% to 73.1% and 18.2%, respectively. Essentially, CoFe funneled CO_2 through CO_2-FTS to olefins, further transformed by HZ-5(40) into aromatics and iso-paraffins. Against a conventional Fe/HZ-5(40) system, CoFe/HZ-5(40) maintained a similar CO_2 conversion rate but reduced CO selectivity, most notably elevating C_{5+} selectivity from 59.0% to 71.5%. This is attributed to CoFe's exceptional ability in CO_2-to-olefins conversion. We also tested the time on stream stability of CoFe/HZ-5(40) for over a 24 hour period and observed that the catalyst exhibited minimal performance degradation after achieving stability (Fig. S6, ESI†).

To probe the CoFe/HZSM-5 tandem system's synergistic effect, we studied zeolite acidity, proximity, and the mass ratio between the components, and their influence on the catalytic system. Zeolite acidity affects aromatization and isomerization, causing different tandem system performances (Fig. 2a and b).

Table 1 Textural and acidic properties of HZSM-5 zeolites

Zeolite	SiO_2/Al_2O_3 [a]	S_{BET} [b] (m^2 g^{-1})	V_{pore} [c] (cm^3 g^{-1})	C_{BAS} [d] (μmol g^{-1})	C_{LAS} [e] (μmol g^{-1})	C_{BAS}/C_{LAS} ratio
HZ-5(40)	45.8	423.3	0.253	61.90	177.14	0.35
HZ-5(80)	91.4	418.3	0.197	32.99	111.38	0.30
HZ-5(160)	187.8	402.5	0.190	22.58	93.13	0.24
HZ-5(320)	353.5	390.4	0.196	8.68	72.52	0.12
HZ-5(640)	682.4	368.4	0.283	3.85	46.72	0.12

[a] SiO_2/Al_2O_3: SiO_2/Al_2O_3 molar ratio by XRF analysis. [b] S_{BET}: specific surface area calculated by the BET method. [c] V_{pore}: total pore volume. [d] C_{BAS}: concentrations of the Brønsted acid site calculated using the Lambert–Beer equation. [e] C_{LAS}: concentrations of the Lewis acid site calculated using the Lambert–Beer equation.

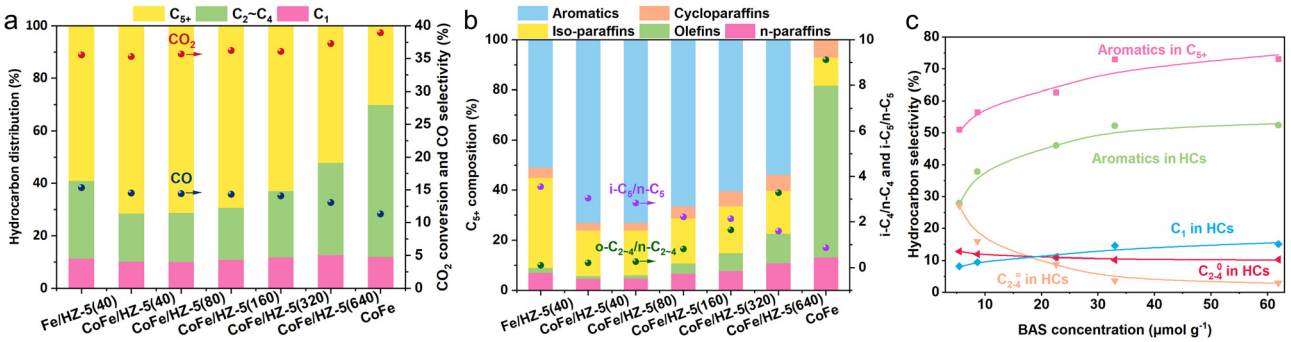

Fig. 2 Hydrocarbon distribution (a) and C_{5+} composition (b) in the case of CO_2 hydrogenation over various catalysts; (c) effect of the BAS concentration on the performance of composite catalysts. N-C_{5+} means C_{5+} hydrocarbons other than aromatics. C^{0}_{2-4} and C_{2-4} denote the paraffins and olefins of C_2–C_4 hydrocarbons, respectively. Reaction conditions: 320 °C, 3.0 MPa, $H_2/CO_2/N_2$ = 72/24/4 (vol%), 4000 mL $g_{cat.}^{-1}$ h^{-1}, time on steam = 14 h.

The BAS, the active site for aromatization, is related to HZSM-5 aromatization capacity.[20] We compared the performances of catalysts with different BAS concentrations using Py-IR technology (Fig. 2c). Increasing the BAS concentration from 3.85 (HZ-5(640)) to 22.58 (HZ-5(160)) μmol g^{-1} boosts aromatic selectivity in C_{5+} hydrocarbons from 53.8% to 73.0%. However, further increases have diminishing returns, suggesting an upper limit for the BAS concentration in promoting aromatic selectivity. At a peak BAS concentration of 61.90 μmol g^{-1}, we achieved the highest C_{5+} aromatic selectivity of 73.1%. As the BAS concentration increased, C_2–C_4 olefin selectivity dropped from 27.3% to 2.8%, while C_2–C_4 paraffin selectivity rose from 8.2% to 15.1%, reducing the olefin/paraffin ratio from 3.3 to 0.2. These changes indicate that the BAS also facilitates olefin hydrogenation, thus increasing paraffin selectivity. Consequently, the BAS concentration is pivotal for selective CO_2 aromatization by the CoFe/HZSM-5 system.

In the CoFe/HZSM-5 catalyst system, the spatial proximity between CoFe and the zeolite is pivotal for their synergistic effects on CO_2-to-C_{5+} hydrocarbon conversion.[21] Three configurations—dual bed, particle mixing, and powder mixing—were used to modulate this spatial relationship (Fig. 3a and b). The dual bed configuration yielded a 34.1% CO_2 conversion rate and 15.9% CO selectivity, with C_{5+} hydrocarbons comprising 67.9% and aromatics making up 62.4% within C_{5+}. Particle mixing enhanced the CO_2 conversion to 35.3% and lowered CO selectivity to 14.5%, while increasing the selectivity for C_{5+} hydrocarbons and aromatics within C_{5+} to 71.5% and 73.1%, respectively. This indicates that reducing the CoFe/HZSM-5 distance promotes olefin diffusion to HZSM-5, benefiting C_{5+} formation. However, close proximity lowered CO_2 conversion to 27.3% and raised CO selectivity. This was probably due to Na ions moving from CoFe to the zeolite acidic sites, poisoning them and altering the catalyst's properties.[5,22]

In the CoFe/HZSM-5 system, the product composition is notably affected by the CoFe/HZSM-5 mass ratio (Fig. 3c and d). Increasing the CoFe/HZSM-5 mass ratio from 0.2 to 0.8 elevates the CO_2 conversion rate from 32.7% to 41.6%, while CO selectivity decreases from 18.1% to 9.4%. Alongside this, the selectivity towards CH_4 shows an increasing trend, scaling from 11.2% to 15.6%, as the CoFe/HZ-5(40) mass ratio ascends from

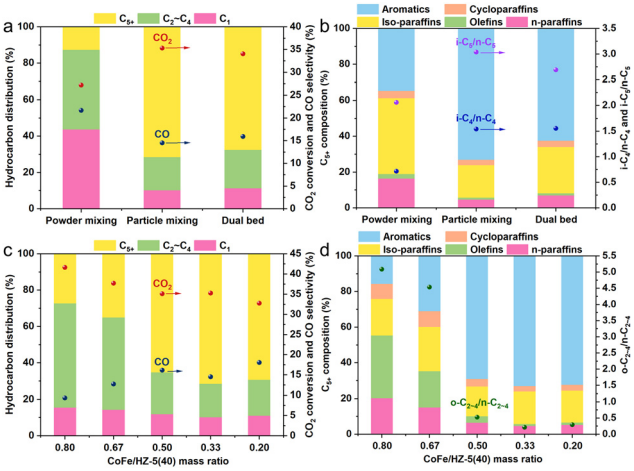

Fig. 3 Hydrocarbon distribution (a) and C_{5+} composition (b) in the case of CO_2 hydrogenation over CoFe/HZ-5(40) with different proximities; hydrocarbon distribution (c) and C_{5+} composition (d) of CO_2 hydrogenation over tandem catalysts with different CoFe/HZ-5(40) mass ratios. Reaction conditions: 320 °C, 3.0 MPa, $H_2/CO_2/N_2$ = 72/24/4 (vol%), 4000 mL $g_{cat.}^{-1}$ h^{-1}, time on steam = 14 h.

0.2 to 0.8. A CoFe/HZSM-5 mass ratio of 0.33 results in the highest C_{5+} hydrocarbon selectivity at 71.5%. Likewise, the ratio of olefins to paraffins in the C_2–C_4 hydrocarbon products surges from 0.3 to 5.1 as the CoFe/HZSM-5 mass ratio increases from 0.2 to 0.8. (Fig. 3d). Specifically, at a CoFe/HZ-5(40) mass ratio of 0.8, the content of aromatic hydrocarbons in the C_{5+} fraction drops to 15.7%, compared to 73.1% at a ratio of 0.33. This contrast highlights the zeolite's pivotal role in olefin oligomerization, isomerization, and aromatization.

Furthermore, an investigation was conducted to analyse the impact of temperature and pressure on the system (Fig. S7a and b, ESI†). The CO_2 hydrogenation process involves a series of multi-step reactions,[23] each with potentially different optimal temperatures. Choosing the right reaction temperature is therefore crucial for enhancing the overall performance. The CO_2 conversion rate escalates from 25.7% to 50.7% as temperature rises from 280 to 380 °C. CH_4 and C_2–C_4 hydrocarbon selectivity

initially drops and then rises, bottoming out at 8.7% and 17.1%, respectively, at 320 °C. Conversely, C_{5+} hydrocarbon selectivity first increases, then decreases, peaking at 74.3% at 320 °C. The ratio of iso-paraffins to normal paraffins in the C_4 and C_5 fractions (i-C_4/n-C_4 and i-C_5/n-C_5) increases gradually with temperature. This suggests that higher temperature enhances the isomerization ability of HZSM-5. In addition, beyond 320 °C, the composition of iso-paraffins and aromatics in the C_{5+} hydrocarbon fraction remains relatively stable despite temperature increases. Based on these findings, it can be concluded that the optimal selectivity for C_{5+} hydrocarbons and minimized CH_4 selectivity were observed at 320 °C.

In CO_2 hydrogenation, the RWGS reaction is isovolumetric, while the FTS reaction decreases the volume, making the overall process volume-reducing. Increasing the pressure aids the forward reaction but also complicates the desorption of products from the catalyst surface. Hence, appropriate reaction pressure is critical for performance optimization. Fig. S7c (ESI†) reveals that upping the pressure boosts the CO_2 conversion rate from 36.8% to 48.1% and diminishes CO selectivity from 16.3% to 4.7%. This effect suggests that both RWGS and FTS benefit from heightened pressure, with a more pronounced impact on FTS, resulting in accelerated intermediate CO conversion and lower by-product CO selectivity. Moreover, Fig. S7d (ESI†) demonstrates the pronounced impact of pressure on hydrocarbon distribution. Specifically, at low pressures, CH_4 selectivity is minimal. However, upon exceeding 3 MPa, CH_4 selectivity notably rises, whereas aromatic selectivity in C_{5+} hydrocarbons takes an inverse trajectory. This indicates a reduced favourability for aromatization at higher pressures. Additionally, as pressure rises, i-C_4/n-C_4 and i-C_5/n-C_5 ratios decline, pointing to adverse effects on zeolite-mediated isomerization.

The CoFe/HZSM-5 tandem catalyst is a highly effective system for the conversion of CO_2 into C_{5+} hydrocarbons. In comparison to the conventional Fe catalyst, the enhanced catalytic activity of the CoFe alloy catalyst facilitates the more efficient conversion of CO_2 to olefins. This heightened efficiency leads to an observed augmentation of intermediate olefins within CoFe/HZ-5(40) as compared to Fe/HZ-5(40), consequently resulting in an increased yield of C_{5+} hydrocarbons. The results clearly show that several factors such as the zeolite acidity, the spatial proximity, the mass ratio of CoFe to HZSM-5, and the specific reaction conditions all play significant roles in determining the performance of the catalyst. Optimizing these factors significantly enhances the selectivity towards C_{5+} hydrocarbons, contributing to the more effective utilization of CO_2 in the production of valuable hydrocarbons.

This work was supported by the National Key R&D Program of China (2022YFA1504700), National Natural Science Foundation of China (22078315), the Youth Innovation Promotion Association of the Chinese Academy of Sciences (2020189), the Natural Science Foundation of Liaoning Province (2022-MS-027), and the Youth Science and Technology Star Project Support Program of Dalian City (2021RQ123), DICP (DICP I202012, DICP I202138).

Conflicts of interest

There are no conflicts to declare.

Notes and references

1 A. Banerjee, G. R. Dick, T. Yoshino and M. W. Kanan, *Nature*, 2016, **531**, 215–219.
2 E. E. Benson, C. P. Kubiak, A. J. Sathrum and J. M. Smieja, *Chem. Soc. Rev.*, 2009, **38**, 89–99.
3 P. Gao, S. Li, X. Bu, S. Dang, Z. Liu, H. Wang, L. Zhong, M. Qiu, C. Yang, J. Cai, W. Wei and Y. Sun, *Nat. Chem.*, 2017, **9**, 1019–1024.
4 P. Gao, S. Dang, S. Li, X. Bu, Z. Liu, M. Qiu, C. Yang, H. Wang, L. Zhong, Y. Han, Q. Liu, W. Wei and Y. Sun, *ACS Catal.*, 2018, **8**, 571–578.
5 J. Wei, Q. Ge, R. Yao, Z. Wen, C. Fang, L. Guo, H. Xu and J. Sun, *Nat. Commun.*, 2017, **8**, 15174.
6 L. Guo, J. Sun, Q. Ge and N. Tsubaki, *J. Mater. Chem. A*, 2018, **6**, 23244–23262.
7 J. Zhu, P. Wang, X. Zhang, G. Zhang, R. Li, W. Li, T. P. Senftle, W. Liu, J. Wang, Y. Wang, A. Zhang, Q. Fu, C. Song and X. Guo, *Sci. Adv.*, 2022, **8**, eabm3629.
8 R. E. Owen, J. P. O'Byrne, D. Mattia, P. Plucinski, S. I. Pascu and M. D. Jones, *Chem. Commun.*, 2013, **49**, 11683–11685.
9 J. Wei, R. Yao, Q. Ge, D. Xu, C. Fang, J. Zhang, H. Xu and J. Sun, *Appl. Catal., B*, 2021, **283**, 119648.
10 J. Wei, R. Yao, Q. Ge, Z. Wen, X. Ji, C. Fang, J. Zhang, H. Xu and J. Sun, *ACS Catal.*, 2018, **8**, 9958–9967.
11 G. T. Kokotailo, S. L. Lawton, D. H. Olson and W. M. Meier, *Nature*, 1978, **272**, 437–438.
12 A. Ramirez, A. Dutta Chowdhury, M. Caglayan, A. Rodriguez-Gomez, N. Wehbe, E. Abou-Hamad, L. Gevers, S. Ould-Chikh and J. Gascon, *Catal. Sci. Technol.*, 2020, **10**, 1507–1517.
13 E. M. Flanigen, J. M. Bennett, R. W. Grose, J. P. Cohen, R. L. Patton, R. M. Kirchner and J. V. Smith, *Nature*, 1978, **271**, 512–516.
14 Y. Li, L. Li and J. Yu, *Chem*, 2017, **3**, 928–949.
15 N. Liu, J. Wei, J. Xu, Y. Yu, J. Yu, Y. Han, K. Wang, J. I. Orege, Q. Ge and J. Sun, *Appl. Catal., B*, 2023, **328**, 122476.
16 L. Zhang, Y. Dang, X. Zhou, P. Gao, A. Petrus van Bavel, H. Wang, S. Li, L. Shi, Y. Yang, E. I. Vovk, Y. Gao and Y. Sun, *The Innovation*, 2021, **2**, 100170.
17 Z. Zeng, Z. Li, L. Kang, X. Han, Z. Qi, S. Guo, J. Wang, A. Rykov, J. Lv, Y. Wang and X. Ma, *ACS Catal.*, 2022, **12**, 6016–6028.
18 K. Y. Kim, H. Lee, W. Y. Noh, J. Shin, S. J. Han, S. K. Kim, K. An and J. S. Lee, *ACS Catal.*, 2020, **10**, 8660–8671.
19 Q. Yang, V. A. Kondratenko, S. A. Petrov, D. E. Doronkin, E. Saraçi, H. Lund, A. Arinchtein, R. Kraehnert, A. S. Skrypnik, A. A. Matvienko and E. V. Kondratenko, *Angew. Chem., Int. Ed.*, 2022, **61**, e202116517.
20 Z. Wan, W. Wu, G. Li, C. Wang, H. Yang and D. Zhang, *Appl. Catal., A*, 2016, **523**, 312–320.
21 Y. Ni, Z. Chen, Y. Fu, Y. Liu, W. Zhu and Z. Liu, *Nat. Commun.*, 2018, **9**, 3457.
22 J. Liu, A. Zhang, X. Jiang, M. Liu, J. Zhu, C. Song and X. Guo, *Ind. Eng. Chem. Res.*, 2018, **57**, 9120–9126.
23 A. Dokania, A. Ramirez, A. Bavykina and J. Gascon, *ACS Energy Lett.*, 2019, **4**, 167–176.

